



Science Arts & Métiers (SAM)

is an open access repository that collects the work of Arts et Métiers Institute of Technology researchers and makes it freely available over the web where possible.

This is an author-deposited version published in: <https://sam.ensam.eu>
Handle ID: <http://hdl.handle.net/10985/20660>

To cite this version :

Mohamed TRABELSI, Eric SEMAIL - Virtual current vectorbased method for inverter openswitch and openphase fault diagnosis in multiphase permanent magnet synchronous motor drives - IET Electric Power Applications - 2021

Any correspondence concerning this service should be sent to the repository

Administrator : scienceouverte@ensam.eu



Virtual current vector-based method for inverter open-switch and open-phase fault diagnosis in multiphase permanent magnet synchronous motor drives

Mohamed Trabelsi¹  | Eric Semail² 

¹National Engineering School of Sousse, University of Sousse, BP 264, Sousse Erriadh, Tunisia

²Univ. Lille, Arts et Metiers Institute of Technology HESAM Université, Centrale Lille, Junia, ULR 2697 - L2EP, F-59000 Lille, France

Correspondence

Mohamed Trabelsi, National Engineering School of Sousse, University of Sousse, BP 264, Sousse Erriadh 4023, Tunisia.
Email: mohamed.trabelsi.mt@gmail.com

Funding information

European Regional Development Fund (ERDF); French State; French Region of Hauts-de-France

Abstract

This paper presents a diagnostic method of inverter open-switch and open-phase faults in multiphase permanent magnet synchronous motor (PMSM) drives. First defined are adequate variables called virtual current vectors. The projection of the zero-sequence current component on these variables was used to define two simple fault indices. High sensitivity to fault is thus induced but with a good robustness to transient states and variation of machine parameters. The mathematical development of the proposed method is provided and supported by experimental tests conducted on two prototypes of multiphase machines in the laboratory: sinusoidal and bi-harmonic PMSMs. The experimental results confirm the effectiveness and the robustness of the proposed method and its capability to detect the single and multiple open-switches and open-phase faults in the electric drive.

1 | INTRODUCTION

Due to its fault tolerant capability, the multiphase machine is a prospective candidate to replace the conventional 3- ϕ machine [1], especially in critical and sensitive applications such as aerospace [2, 3], automotive [4, 5], and marine applications [6]. The multiphase machine is naturally fault tolerant since a rotating field can be generated even in postfault operation mode. However, some effects such as high current/voltage peaks and torque ripples may be unbearable in applications. For example, the inverter open-circuit fault is one of the prevalent electrical faults in alternating current (ac) motor drives [7]. If this fault is not detected in its earliest stage, it leads to mechanical vibrations and thermal stress, fostering progressive degradation of other components of the system [8].

In order to ensure safe and continuous operation of the electric drive, the fault tolerant control strategies should be applied as fast as possible to keep the highest possible average torque with low levels of ripples and losses. In the literature, several fault tolerant control techniques have been investigated, as addressed in [9–14]. It is obvious that the real-time implementation of these techniques requires essentially the accurate

information provided by the diagnostic step, which should also be achieved as fast as possible.

This paper focuses on the diagnosis of open-switch and open-phase faults in the voltage source inverter (VSI) feeding ac machines. There are many instructive papers that have addressed the problem of real-time detection and identification of these faults. The proposed fault detection and identification (FDI) processes in the literature include real-time estimation-based models [15–19], current signals-based methods [20–23], or voltage signals-based methods [24–26]. These strategies are well known and references [8, 27] give a more comprehensive bibliography, especially for the classical three-phase electric drives.

However, many of the prior methods [15–19] have seen limitations in terms of practicality in the case of multiphase drives. For instance, the robustness of the model-based methods is dependent on the accuracy of the model parameters estimation. On the other hand, taking into account the multimachines concept of the multiphase drives, these methods involve at least two 2D machine models and a large number of parameters. In turn, this results in low robustness and more complexity of the real-time FDI process implementation. Moreover the higher the number of phases, the lower the

This is an open access article under the terms of the Creative Commons Attribution-NonCommercial-NoDerivs License, which permits use and distribution in any medium, provided the original work is properly cited, the use is non-commercial and no modifications or adaptations are made.

© 2021 The Authors. *IET Electric Power Applications* published by John Wiley & Sons Ltd on behalf of The Institution of Engineering and Technology.

impact of a fault with, as a consequence, a higher difficulty to detect the fault.

References [20, 21] proposed current signals-based inverter open-switch fault diagnostic methods in the case of sinusoidal three-phase permanent magnet synchronous motors (PMSMs). However, while working with multiphase PMSM drives, these strategies may not be effectively applied since multiple harmonic components (3rd, 5th, 7th, etc.) can be involved in the back- electromotive forces (EMFs), such as the case of biharmonic machines addressed in [28–30]. As expected in [30, 31], the asymmetrical distribution of the fault current quantities in the healthy phases after the fault occurrence leads to large nonzero values of all fault indices. In turn, this can cause false alarms in the FDI process.

It was only recently that real-time detection methods in multiphase electric drives have been investigated in the literature, as addressed in [30–34]. In [32], a current signal-based model identification method is used to detect open-switch and open-phase faults occurrence in a brushless direct current five-phase PMSM supplied by the first and third current harmonics. An adaptive recursive least square (RLS) identification is used to identify the current signals and then to generate the signal errors between the output of adaptive estimation and the one obtained by the model. However, in addition to the model parameter dependency, the use of an adaptive estimator for each phase greatly increases the computation time.

Taking advantage of the multimachine concept, it is possible to define a robust FDI process to detect the inverter open-circuit fault occurrence in the multiphase drives. In fact, in [10, 31, 33–35], for sinusoidal multiphase machines, it is highlighted that an open-switch or an open-phase fault results in a fault current component appearing in the x - y frame instead of a zero current value in normal operation mode. Accordingly, the method investigated in [33] uses a centroid-approach to identify the direction of the fault component for fault detection. A similar diagnostic principle is extended to multiphase induction machines using a time-domain current-based approach, as addressed in [31, 34]. These strategies are successfully applied for sinusoidal machines supplied by sinusoidal currents when the x - y current components are zero in normal conditions. However, for the biharmonic multiphase machines (with nonsinusoidal excitation), as addressed in [28–30], the x - y current components exist also when the electric drive operates free of any fault. Consequently, the methods presented in [31, 33, 34] cannot be applied to the biharmonic multiphase PMSMs.

The fault diagnosis problem in the case of the biharmonic multiphase PMSM is addressed in [30]. In addition to the existing frames α - β and x - y designed for the control, the authors defined a new frame, called fault reference frame, designed only for the fault diagnosis. Then, fault indices are defined based on the particular shape of the fault trajectory in the fault reference frame. The diagnostic method is applied to Y-connected windings without neutral. However, this method is not suitable for the diagnosis of the open-switch faults in the case of electric drives owning a path for the circulating zero-sequence (ZS) current.

Only few studies addressed the problem of inverter open-circuit fault for the topologies owning a path for the ZS

current component. These topologies regroup the Δ -connected windings, the Y-connected windings with neutral connected to the direct current (dc)-link midpoint, and the open-end windings PMSM with common dc-link. In [36], the authors proposed an open-phase fault detection method for the Δ -connected 3- ϕ PMSM. A fault index, derived from the zero-sequence current component (ZSCC), and auxiliary variables derived from phase currents are all used to detect and locate the faulty phase. Unfortunately, the defined fault indices are limited to the open-phase fault case and they are not able to detect and locate an open-switch fault in the VSI.

In [37], for the parallel inverters system, the ZSCC is used to detect the open-switch fault. However, as concluded by the authors, the proposed method is totally related to the absence of the circulating current components under healthy conditions. This is not ensured in practice since a circulating current can exist depending on the pulse width modulation (PWM) technique used [38, 39].

Based on the preceding discussion, this paper proposes a simple inverter open-circuit fault diagnostic method in multiphase electric drives. The proposed method allows overcoming the limitations of the existing strategies and is further verified by experimental tests. The main contributions of this paper are as follows:

Variables called virtual current vectors (V_{CV_n}) are defined from the data available in α - β and x - y frames, and they are dedicated only for fault diagnosis purposes. These variables as well as the ZSCC are used as inputs of the real-time FDI process. The diagnostic principle consists of a direct projection of the ZSCC onto the defined V_{CV_n} . Two simple fault indices are then defined and permitted to detect and identify the single and multiple open-switches and open-phase faults in the electric drive. The theoretical development of this approach is given here to support the proposed idea.

The proposed method permits the detection of open-circuit inverter fault for both sinusoidal and biharmonic multiphase PMSMs.

The proposed method is derived from the ZSCC, which presents a weak value in prefault operation mode and coincides with V_{CV_n} in postfault operation mode. Owing to these features, the robustness of the FDI process does not depend on the fast transient states induced by load and speed changes.

The experimental tests in the laboratory are conducted on two five-phase PMSM prototypes: sinusoidal PMSM and biharmonic PMSM (supplied normally by two significant current harmonics in maximum torque per ampere [MTPA] operation mode). The obtained results confirm the effectiveness and the robustness of the proposed method and its capability to detect the single and multiple open-switch and open-phase faults.

The paper is organised as follows. The theory behind the proposed method and the derivation of the V_{CV_n} variables are presented in Section 2. Section 3 discusses the procedure of

the fault diagnostic strategy using the VCV_n and the ZSCC. The experimental test rig and the obtained results conducted on two five-phase PMSM prototypes are provided in Section 4 to verify the effectiveness and the robustness of the proposed real-time FDI process.

2 | VIRTUAL CURRENT VECTORS DERIVATION

2.1 | Theoretical principle

The basic idea of the proposed approach is based upon the phase currents imbalance upon occurrence of an open-switch fault of any of the inverter legs. When considering only the low order current harmonic components (1st and 3rd harmonics), the motor phase currents can be written as

$$i_n(t) = I_{r1} \sin\left(p\Omega t - (n-1)\frac{2\pi}{5}\right) - I_{r3} \sin\left(3\left(p\Omega t - (n-1)\frac{2\pi}{5}\right)\right) \quad (1)$$

where $n = \{1, 2, 3, 4, 5\}$ denotes the motor phase currents ($i_a, i_b, i_c, i_d,$ and i_e), respectively. I_{r1} and I_{r3} denote the magnitudes of the current harmonic components, and $p\Omega$ is the electrical fundamental frequency.

Then, the sum of the phase currents gives the ZS component

$$i_{zsc}(t) = i_a(t) + i_b(t) + i_c(t) + i_d(t) + i_e(t). \quad (2)$$

Assuming no PWM switching effect, no parameter temperature dependence (balanced excitation), and no fault in the electric drive, the sum of the phase currents must be zero regardless of the connection mode of the motor windings. That is,

$$i_{zsc}(t) = 0. \quad (3)$$

In the presence of open-switch or open-phase fault in the VSI, Equation (3) presents a nonzero value, where

$$i_{zsc}(t) \neq 0 \quad (4)$$

shows typical characteristic in postfault operation mode for any stator winding configuration owning a path for the ZS current component, including the Δ -connected PMSM, the Y-connected PMSM with neutral connected to the dc-link midpoint, and the open-end windings PMSM with common dc-link. The considered configurations of the stator windings are summarised in Figure 1.

The motor phase currents, i_a, i_b, i_c, i_d and i_e can be expressed in terms of the vector space decomposition (VSD)

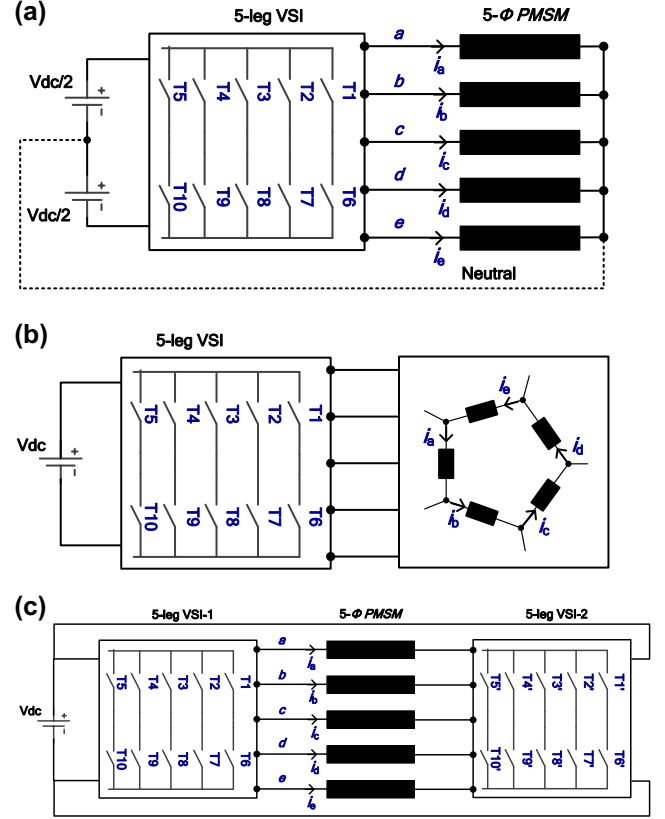


FIGURE 1 Stator windings configurations. (a) Y-connected permanent magnet synchronous motor (PMSM) with neutral connected to the dc-link midpoint; (b) Δ -connected PMSM; (c) open-end windings PMSM with common dc-link. VSI, voltage source inverter

variables using the inverse of the power-invariant Concordia transformation matrix H^{-1} :

$$H^{-1} = \sqrt{\frac{2}{5}} \begin{bmatrix} 1 & 0 & 1 & 0 & \frac{1}{\sqrt{2}} \\ \cos\frac{2\pi}{5} & \sin\frac{2\pi}{5} & \cos\frac{4\pi}{5} & \sin\frac{4\pi}{5} & \frac{1}{\sqrt{2}} \\ \cos\frac{4\pi}{5} & \sin\frac{4\pi}{5} & \cos\frac{8\pi}{5} & \sin\frac{8\pi}{5} & \frac{1}{\sqrt{2}} \\ \cos\frac{6\pi}{5} & \sin\frac{6\pi}{5} & \cos\frac{12\pi}{5} & \sin\frac{12\pi}{5} & \frac{1}{\sqrt{2}} \\ \cos\frac{8\pi}{5} & \sin\frac{8\pi}{5} & \cos\frac{16\pi}{5} & \sin\frac{16\pi}{5} & \frac{1}{\sqrt{2}} \end{bmatrix}$$

$$[i_a \ i_b \ i_c \ i_d \ i_e] = H^{-1} [i_\alpha \ i_\beta \ i_x \ i_y \ i_b]^T \quad (5)$$

where $[i_\alpha, i_\beta, i_x, i_y, i_b]$ represent the equivalent current components in α - β , x-y, and ZS frames.

Taking into account the condition that the motor phase current $i_n = 0$, $n = \{a, b, c, d, e\}$, and expressing the currents of the remaining healthy phases by their equivalent VSD variables allow calculating the exact expression of the ZSCC i_{zsc} .

For illustration, in the case of an open-circuit fault of the motor phase a, the ZSCC is defined as

$$i_{zsc} |_{i_a=0} = i_b + i_c + i_d + i_e \quad (6)$$

by expressing i_b, i_c, i_d and i_e by their VSD variables, it yields

$$i_{zsc} |_{i_a=0} = -\sqrt{\frac{2}{5}}(i_\alpha + i_x) + \frac{4}{\sqrt{5}}i_b \quad (7)$$

where i_b is the equivalent current component in the ZS frame derived from the power-invariant matrix given in Equation (5). It is expressed by

$$i_b = \frac{1}{\sqrt{5}}i_{zsc} \quad (8)$$

substituting Equation (8) into Equation (7) results in

$$i_{zsc} |_{i_a=0} = -\sqrt{10}(i_\alpha + i_x) \quad (9)$$

The same analysis can be extended to the remaining cases. Therefore, it can be proven that the general expression of the ZSCC i_{zsc} can be given by

$$\begin{aligned} i_{zsc} = & -\sqrt{10} \left(\cos \left((n-1) \frac{2\pi}{5} \right) i_\alpha + \sin \left((n-1) \frac{2\pi}{5} \right) i_\beta \right. \\ & \left. + \cos \left(2(n-1) \frac{2\pi}{5} \right) i_x + \sin \left(2(n-1) \frac{2\pi}{5} \right) i_y \right) \end{aligned} \quad (10)$$

where $n = 1, 2, 3, 4,$ or 5 when the fault occurs in the motor phase a, b, c, d, or e, respectively.

The relationship (Equation (10)) between i_{zsc} and the current components $i_{\alpha\beta}, i_{xy}$ is interesting because the first term, i_{zsc} , exists only under a fault condition and it is equal to zero when the electric drive operates free of any fault. However, the second term, as it is a function of $i_{\alpha\beta}$ and i_{xy} , it is always varying regardless the operation mode of the electric drive. Hence, the second term will be used to represent the virtual current vectors VCV_n and then to compare with the measured ZSCC i_{zsc} for fault diagnosis purposes. In the rest of the paper, VCV_n are given by

$$\begin{aligned} VCV_n = & -\sqrt{10} \left(\cos \left((n-1) \frac{2\pi}{5} \right) i_\alpha + \sin \left((n-1) \frac{2\pi}{5} \right) i_\beta \right. \\ & \left. + \cos \left(2(n-1) \frac{2\pi}{5} \right) i_x + \sin \left(2(n-1) \frac{2\pi}{5} \right) i_y \right) \end{aligned} \quad (11)$$

As the PMSM is fed by a five-leg VSI, five virtual current vectors, denoted by $(VCV_1, VCV_2, VCV_3, VCV_4, VCV_5)$, are

defined. Using these quantities and according to the fault location, the ZSCC i_{zsc} is expressed as follows:

- If an open-phase fault occurs in phase n,

$$i_{zsc}(t) = VCV_n, \text{ for } 0 \leq p\Omega t \leq 2\pi \quad (12)$$

- If an open-switch fault occurs to the upper bridge of phase n,

$$i_{zsc}(t) = \begin{cases} VCV_n, & \text{for } (n-1) \frac{2\pi}{5} \leq p\Omega t \leq \pi + (n-1) \frac{2\pi}{5} \\ 0, & \text{for } \pi + (n-1) \frac{2\pi}{5} \leq p\Omega t \leq 2\pi + (n-1) \frac{2\pi}{5} \end{cases} \quad (13)$$

- If an open-switch fault occurs to the lower bridge of phase n,

$$i_{zsc}(t) = \begin{cases} 0, & \text{for } (n-1) \frac{2\pi}{5} \leq p\Omega t \leq (n-1) \frac{2\pi}{5} + \pi \\ VCV_n, & \text{for } \pi + (n-1) \frac{2\pi}{5} \leq p\Omega t \leq 2\pi + (n-1) \frac{2\pi}{5} \end{cases} \quad (14)$$

In order to get a better understanding of the dynamic of the VCV_n and i_{zsc} in prefault and postfault operation modes, a simulation step is performed on a biharmonic five-phase PMSM. The rotor speed and the load torque are fixed at 1000 rpm and 10 N.m, respectively. The third current harmonic I_{r3} is fixed to 25% of the fundamental harmonic I_{r1} .

As shown in Figure 2, when the fault occurs, the phase current i_n drops constantly to zero during the current period if the fault is an open-phase (see Figure 2a), and it is limited to flow only in the negative or positive directions over a half current period if the fault is an open-switch (see Figure 2b). The ZSCC i_{zsc} flows in positive or/and negative directions instead of a zero value obtained in prefault operation mode.

Simulation results depicted in Figure 3 provide the dynamic of i_{zsc} and VCV_n during the fault occurrence in the VSI. As predicted in Equations (12)–(14), i_{zsc} is equal to zero in prefault operation mode and coincides with VCV_n in postfault operation mode. Based on this feature, the next sections discuss the main steps required to find a simple diagnostic algorithm derived from the defined virtual current vectors VCV_n and the ZSCC i_{zsc} .

2.2 | Practical considerations

In practice, the zero value of the ZSCC given by Equation (3) is never achieved. A weak value can be caused by a phase impedance disturbance, by high order switching harmonics, or by sensors and instrumentation errors. In this work, it is assumed that the weak value of i_{zsc} can be neglected in normal operation mode compared to its value under fault conditions. On the other side, it can be proven that the proposed

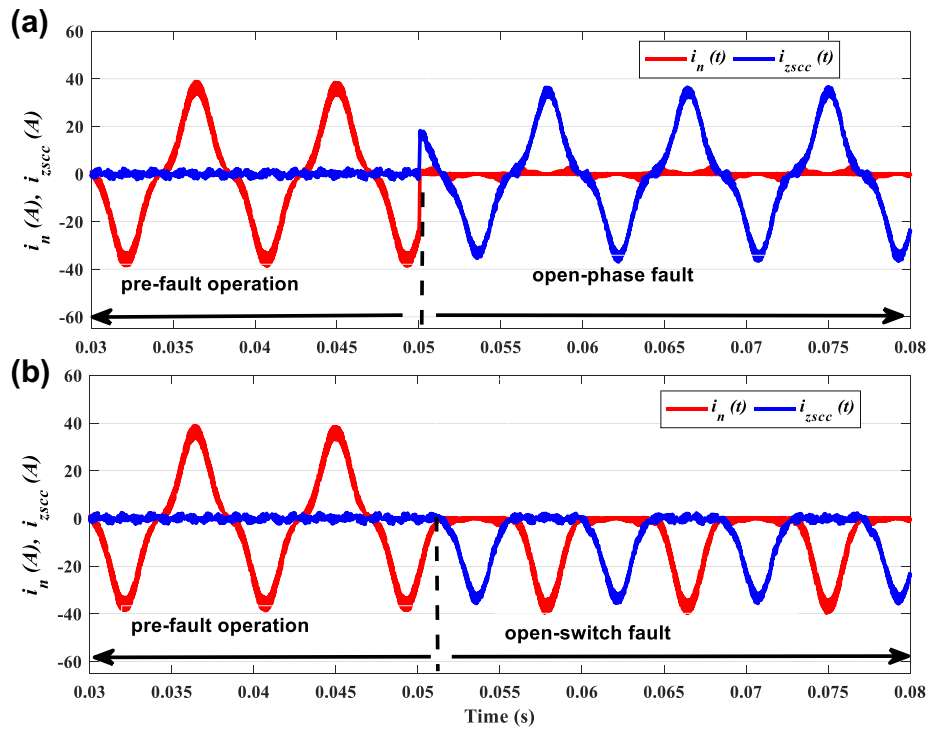


FIGURE 2 Simulation results. Time-domain waveforms of the phase current $i_n(t)$ and the zero-sequence current component i_{zsc} in pre-fault and post-fault operation mode of the electric drive. (a) open-phase fault and (b) open-switch fault

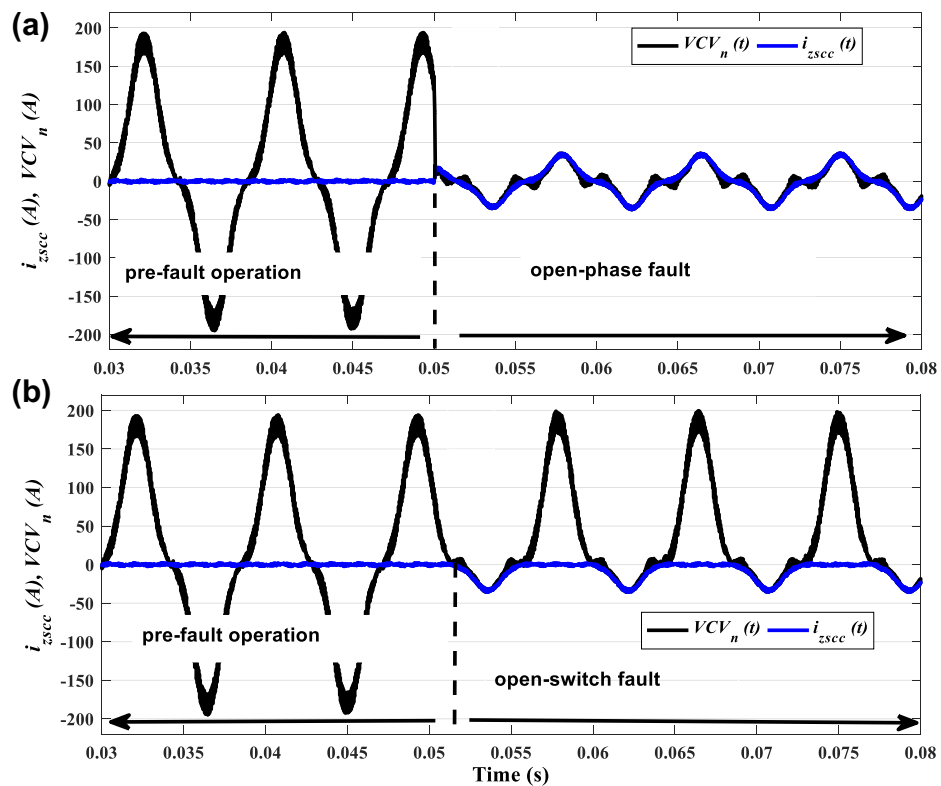


FIGURE 3 Simulation results. Time-domain waveform of the zero-sequence current component i_{zsc} and the virtual current vectors (VCV_n) in pre-fault and post-fault operation mode of the electric drive. (a) open-phase fault and (b) open-switch fault

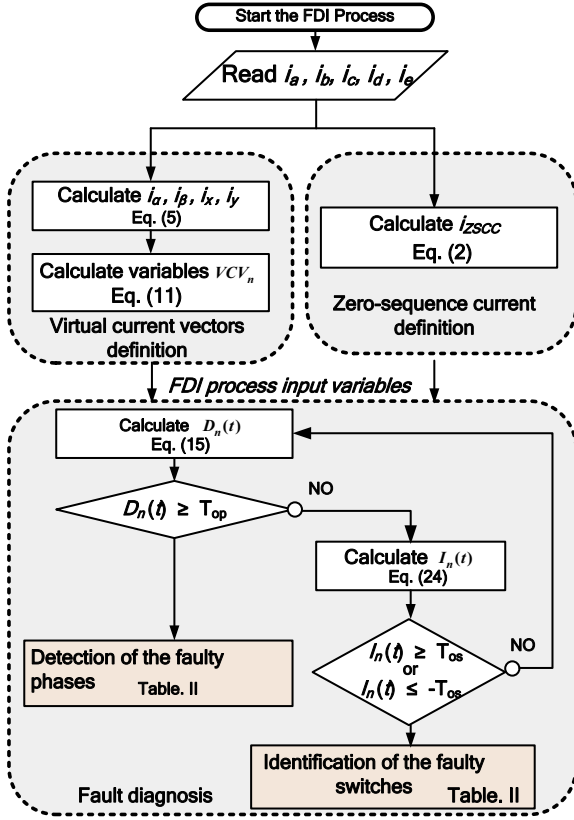


FIGURE 4 Flowchart of the proposed real-time fault detection and identification (FDI) process

diagnostic method can be used even if the ZSCC is not strictly equal to zero in normal operation mode (these assertions are illustrated and analysed in the sequel with some experimental results).

3 | VIRTUAL CURRENT VECTOR-BASED REAL-TIME FDI PROCESS

In the previous sections, the objective was to obtain interesting variables that can be used as inputs to the real-time FDI process. The objective is to obtain robust fault indices that allow the detection and identification of open-switch and open-phase faults without causing false alarms.

The proposed real-time FDI process is illustrated in the flowchart of Figure 4. It consists of detecting and identifying open-switch and open-phase faults. The measured quantities used by this algorithm are only the motor phase currents and the actual rotor speed that are already used for a closed-loop control of the five-phase PMSM.

3.1 | Open-phase fault detection procedure

For open-phase fault detection, a variable such as (i_{zSCC}/VCV_n) , which is equal to 1 in postfault operation mode, seems interesting. However, in pre-fault operation mode, its zero value

is not assured because of the zero-crossing of VCV_n during short durations (see Figure 3). In order to alleviate this problem and to keep a value equal to one always in fault mode, it is proposed here to replace the ratio (i_{zSCC}/VCV_n) by its average absolute value, resulting in the following diagnostic variables:

$$D_n(t) = \frac{\langle |i_{zSCC}| \rangle (t)}{\langle |VCV_n| \rangle (t)} \quad (15)$$

with

$$\langle |x| \rangle (t) = \frac{1}{T(t)} \int_{z=t-T(t)}^{z=t} |x|(z) dz \quad (16)$$

where $\langle . \rangle$ and $\langle | . | \rangle$ denote the average value and the average absolute values, respectively. X represents the variable i_{zSCC} or VCV_n , and $T(t)$ is the sliding window used, which is defined from the instantaneous actual measured rotor speed $\Omega(t)$ as follows:

$$T(t) = \frac{2\pi}{p\Omega(t)} \quad (17)$$

In pre-fault operation mode, the current components in α - β and x-y frames are sinusoidal. Those are

$$i_{\alpha\beta}(t) = \begin{cases} \sqrt{5/2}I_{r1} \sin(p\Omega t) \\ \sqrt{5/2}I_{r1} \sin\left(p\Omega t - \frac{\pi}{2}\right) \end{cases} \quad (18)$$

$$i_{xy}(t) = \begin{cases} \sqrt{5/2}I_{r3} \sin(-3p\Omega t) \\ \sqrt{5/2}I_{r3} \sin\left(-3\left(p\Omega t - \frac{\pi}{2}\right)\right) \end{cases} \quad (19)$$

Following this and using Equations (11) and (16), the variable $\langle |VCV_n| \rangle$ can be calculated as given in Equation (20).

$$\begin{aligned} \langle |VCV_n| \rangle (t) = \frac{1}{T(t)} \int_{z=t-T(t)}^{z=t} & \left| \sqrt{10} \left(\cos\left((n-1)\frac{2\pi}{5}\right) i_\alpha \right. \right. \\ & + \sin\left((n-1)\frac{2\pi}{5}\right) i_\beta + \cos\left(2(n-1)\frac{2\pi}{5}\right) i_x \\ & \left. \left. + \sin\left(2(n-1)\frac{2\pi}{5}\right) i_y \right) \right| dz \end{aligned} \quad (20)$$

The average absolute value of VCV_n is a combination of the current components $i_{\alpha\beta}$ and i_{xy} , themselves a function of the magnitudes of the first harmonic I_{r1} and the third harmonic I_{r3} , respectively. Considering the MTPA strategy applied

to the PMSM, I_{r3} can be expressed simply as a fraction of I_{r1} as follows:

$$I_{r3} = \rho I_{r1} \quad (21)$$

According to the ρ value, two cases have to be considered. Each case has a $\langle |V_{CV_n}| \rangle$ value given by the following:

- In case_01: sinusoidal or almost sinusoidal 5 – ϕ PMSM;
 $\rho \in \left[0; \frac{1}{3}\right]$

$$\langle |V_{CV_n}| \rangle (t) = \frac{10}{\pi} I_{r1} \left(1 - \frac{1}{3}\rho\right) \quad (22)$$

- In case_02: biharmonic (nonsinusoidal) 5 – ϕ PMSM;
 $\rho \in \left]\frac{1}{3}; +\infty\right[$

$$\langle |V_{CV_n}| \rangle (t) = \frac{10}{\pi} I_{r1} \left(\frac{2}{3}(1+\rho)\left(1+\frac{1}{\rho}\right)^{1/2} + \frac{1}{3}\rho - 1\right) \quad (23)$$

Regardless of the ρ value, it can be proven that the diagnostic variables D_n are close to zero when the VSI operates free of any fault since i_{ZSCC} assumes zero value in this mode. However, when an open-phase fault occurs in the VSI, i_{ZSCC} coincides with V_{CV_n} . Taking this into account and considering Equations (22) and (23), D_n will converge to +1. The fault occurrence is judged when D_n crosses a fixed threshold T_{op} . Table 1 summarises the D_n variable states according to the faulty phase location in the 5- ϕ PMSM.

3.2 | Open-switch fault identification procedure

The diagnostic variables defined in Equation (15) carry information only about the open-phase fault occurrence. In order to achieve a complete fault diagnosis, the proposed FDI process is extended to open-switch fault identification. Once more, based on the ZSCC i_{ZSCC} and the V_{CV_n} , the identification variables are defined as follows:

$$I_n(t) = \frac{\langle V_{CV_n} - i_{ZSCC} \rangle (t)}{\langle |V_{CV_n}| - |i_{ZSCC}| \rangle (t)} \quad (24)$$

In normal operation mode, i_{ZSCC} is equal to zero and V_{CV_n} assumes a symmetrical alternating waveform with zero average value. This gives as a result zero value of the identification variables I_n .

When an open-switch fault occurs in the VSI, the ZSCC i_{ZSCC} will present positive or negative direction according to the

fault location. In addition, i_{ZSCC} will be equal to V_{CV_n} over only half a current period, as depicted in Figure 3(b). As a consequence, the quantity $(|V_{CV_n}| - |i_{ZSCC}|)$ always assumes positive values. On the other hand, the quantity $(V_{CV_n} - i_{ZSCC})$ assumes positive or negative values according to the fault location. Taking this into account and using Equations (13), (14), and (16), over a fundamental current period, the identification variable in Equation (24) can be rewritten as follows:

- If an open-switch fault occurs to the upper bridge of phase n,

$$I_n(t) = \frac{\frac{1}{T(t)} \int_{z=t-T(t)}^{z=t} (V_{CV_n} - i_{ZSCC})(z) dz}{\frac{1}{T(t)} \int_{z=t-T(t)}^{z=t} (|V_{CV_n}| - |i_{ZSCC}|)(z) dz} \quad (25.a)$$

Computing Equation (25.a), it yields

$$I_n(t) = \begin{cases} \frac{\frac{5}{\pi} I_{r1} \left(1 - \frac{1}{3}\rho\right)}{\frac{5}{\pi} I_{r1} \left(1 - \frac{1}{3}\rho\right)} = +1, & \text{if } \rho < \frac{1}{3} \\ \frac{\frac{5}{\pi} I_{r1} \left(-1 + \frac{1}{3}\rho + \frac{2}{3}(1+\rho)\left(1 + \frac{1}{\rho}\right)^{1/2}\right)}{\frac{5}{\pi} I_{r1} \left(-1 + \frac{1}{3}\rho + \frac{2}{3}(1+\rho)\left(1 + \frac{1}{\rho}\right)^{1/2}\right)} = +1, & \text{if } \rho > \frac{1}{3} \end{cases} \quad (25.b)$$

- If an open-switch fault occurs to the lower bridge of phase n,

$$I_n(t) = \frac{\frac{1}{T(t)} \int_{z=t-T(t)}^{z=t} (V_{CV_n} - i_{ZSCC})(z) dz}{\frac{1}{T(t)} \int_{z=t-T(t)}^{z=t} (|V_{CV_n}| - |i_{ZSCC}|)(z) dz} \quad (26.a)$$

Computing Equation (26.a), it yields

$$I_n(t) = \begin{cases} \frac{-\frac{5}{\pi} I_{r1} \left(1 - \frac{1}{3}\rho\right)}{\frac{5}{\pi} I_{r1} \left(1 - \frac{1}{3}\rho\right)} = -1, & \text{if } \rho < \frac{1}{3} \\ \frac{-\frac{5}{\pi} I_{r1} \left(-1 + \frac{1}{3}\rho + \frac{2}{3}(1+\rho)\left(1 + \frac{1}{\rho}\right)^{1/2}\right)}{\frac{5}{\pi} I_{r1} \left(-1 + \frac{1}{3}\rho + \frac{2}{3}(1+\rho)\left(1 + \frac{1}{\rho}\right)^{1/2}\right)} = -1, & \text{if } \rho > \frac{1}{3} \end{cases} \quad (26.b)$$

It is clear that the identification variables I_n converge to +1 or -1 according to the open-switch fault location and regardless of the nature of the multiphase PMSM (with sinusoidal or nonsinusoidal back-EMF). Table 1 summarises the

TABLE 1 Diagnostic variables states in prefault and postfault operation modes

	ZSCC i_{ZSCC}	Duration of i_{ZSCC}	Detection variables D_n	Identification variables I_n
Prefault mode	$= 0$	Over fundamental period	$= 0$	$= 0$
Open-switch fault	Upper bridge	Over positive half current cycle, Equation (13)	$= 0$	$\geq T_{OS}$
	Lower bridge	Over negative half current cycle, Equation (14)	$= 0$	$\leq -T_{OS}$
Open-phase fault	Upper and lower bridge	Over fundamental period, Equation (12)	$\geq T_{OP}$	$= 0$

states of the variables I_n according to the faulty switch location in the VSI. The fault occurrence is judged when I_n crosses a fixed threshold T_{OS} .

3.3 | Thresholds selection in the FDI process

Generally, the robustness and the immunity of an FDI process against false alarms are very dependent on the selected threshold values used for fault detection. In this work, there are only two threshold values used, T_{OP} and T_{OS} , respectively, for open-phase fault and open-switch fault diagnosis. These values are selected by taking into account several factors that impact the evolution of the diagnostic variables D_n and I_n . These factors are the transient states induced by the load torque and the motor speed change, the switching and the sensors noises, and the different levels that can be taken by the variables D_n and I_n in prefault and postfault operation modes.

The proposed real-time FDI process is derived from the ZSCC, which presents a weak value in prefault operation mode and coincides with V_{CV_n} in postfault operation mode. Owing to these features, the robustness of the FDI process does not depend on the fast transient states induced by load and speed changes. In addition, the sliding window $T(t)$ (see Equation (17)) used to calculate the average values acts as a low pass filter. This results in a weak effect of the switching and sensors noises on the diagnostic variables.

The value of the threshold T_{OP} is selected by considering the behaviour of the variables D_n in normal operation mode and under faulty conditions. Theoretically, the variable D_n is equal to 0 or 1 in these two cases. This means that the threshold T_{OP} is between 0 and 1. However, a ZSCC can exist according to the PWM technique used. Several modulation strategies are used for eliminating the common mode current (CMC) in normal operation mode [39]. But here, it can be proven that the proposed technique in this paper is independent of the used PWM strategy and can be used even with the conventional sinus-triangle modulation strategy.

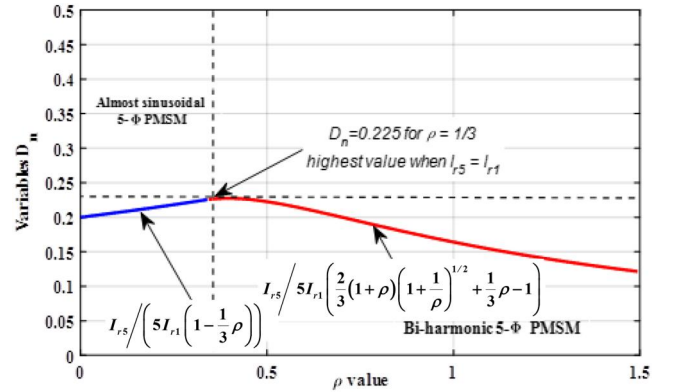


FIGURE 5 Variation of the diagnostic variables D_n according to the ρ value when $I_{r5} = I_{r1}$ (prefault operation mode)

Beyond this, assuming that a ZSCC can exist in a healthy operation mode of the 5- ϕ PMSM, it can be expressed by

$$i_{ZSCC}(t) = I_{r5} \sin(5p\Omega t) \quad (27)$$

Substituting Equation (27) into Equation (15) and taking into account Equations (22) and (23) gives the expression of the variables D_n in normal operation mode:

$$D_n = \begin{cases} \frac{I_{r5}}{5I_{r1} \left(1 - \frac{1}{3}\rho\right)}, & \text{if } \rho < \frac{1}{3} \\ \frac{I_{r5}}{5I_{r1} \left(\frac{2}{3}(1+\rho) \left(1 + \frac{1}{\rho}\right)^{1/2} + \frac{1}{3}\rho - 1\right)}, & \text{if } \rho > \frac{1}{3} \end{cases} \quad (28)$$

Figure 5 illustrates the variation of D_n according to the ρ value in normal operation mode. Theoretically, the highest value of 0.225, which can be taken by D_n in normal conditions, is reached when $I_{r5} = I_{r1}$ and $\rho = 1/3$. Accordingly, a threshold value, bigger than 0.225, permits the rejection of the ZSCC effects. In practice, it is verified that a weak CMC is induced in

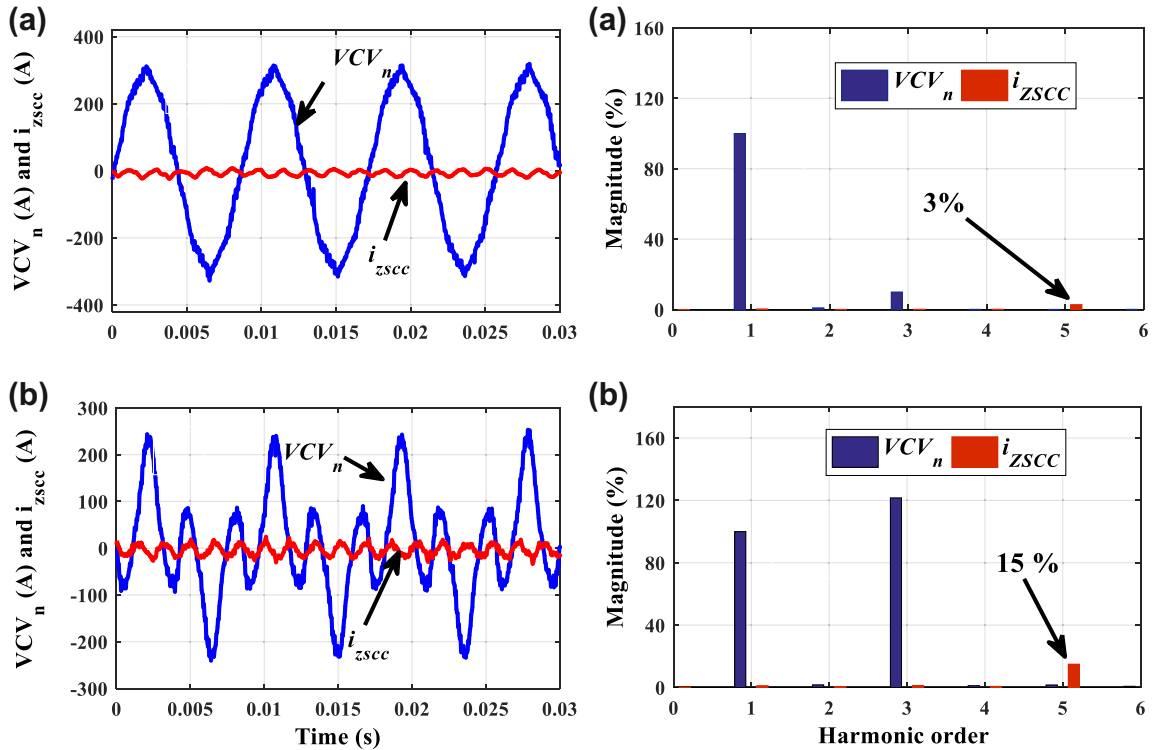


FIGURE 6 Experimental results. Time-domain waveforms of the virtual current vectors VCV_n , the zero-sequence current component (ZSCC) i_{zsc} and their harmonic content. (a) Sinusoidal 5- ϕ permanent magnet synchronous motor prototype; (b) biharmonic 5- ϕ permanent magnet synchronous motor prototype

the ZS plane, as shown in Figure 6. The current i_{zsc} has its highest value equal to 15% in comparison to VCV_n in the case of a biharmonic PMSM (3% for the sinusoidal one). This gives as a result a value of D_n close to 0.06. Accordingly, T_{op} is selected equal to a

universal value of 0.45, resulting in a better trade-off between the fault detection speed and the immunity against false alarms.

With similar reasoning, the threshold T_{os} is selected, taking into account the behaviour of the diagnostic variables I_n in pre-fault and post-fault operation modes. These variables are equal to zero when the VSI operates free of any fault and equal to ± 1 when an open-switch fault occurs in the VSI. In normal operation mode, there is no effect of the CMC on the variables I_n since they are computed based on average values. Accordingly, the threshold T_{os} is fixed to 0.5.

4 | EXPERIMENTAL RESULTS

4.1 | Experimental platform

The different elements of the experimental platform that has been used for the real-time FDI process evaluation are shown in Figure 7 and Figure 8. The tests are carried out on two five-phase PMSM prototypes: a sinusoidal PMSM supplied with sinusoidal current, and a biharmonic PMSM supplied with two

significant current harmonics (1st and 3rd harmonics). The main parameters of the used PMSMs are shown in Table 2. The open-end windings configuration given in Figure 1(c) is under investigation. Therefore, two five-leg VSIs, operating at 15 kHz switching frequency, are used to drive the PMSMs. The VSIs are connected to a common dc-bus voltage of 48 V, and are interfaced with a digital control board based on a dSPACE DS1006 running with an execution step time of 40 μ s. An industrial motion drive is coupled to the shaft of the 5- ϕ PMSM. It is used as an emulator to generate different load profiles.

Here, it is important to underline that the open-end windings configuration is used for experimental investigation but the same results can be obtained for any stator winding configuration shown in Figure 1.

4.2 | Experimental tests

Five tests confirm the robustness of the diagnostic algorithm under healthy conditions, and its capability to detect and identify the open-phase and open-switch faults in the case of sinusoidal and nonsinusoidal current supply:

- **Test 1** – FDI process immunity against speed change: This test is performed on the biharmonic 5- ϕ PMSM prototype. A constant load of 20 N.m is applied to the motor under MTPA control strategy, keeping I_{r3} equal to $1.22 \times I_{r1}$

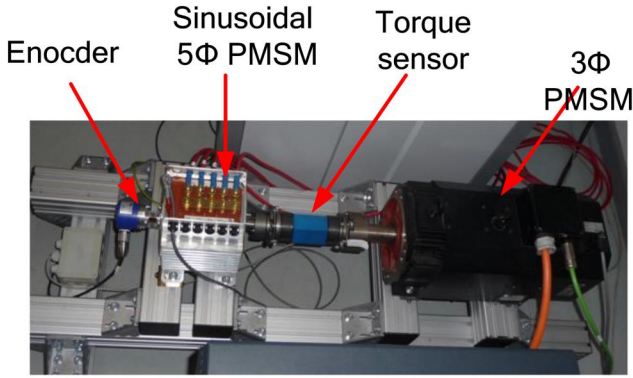
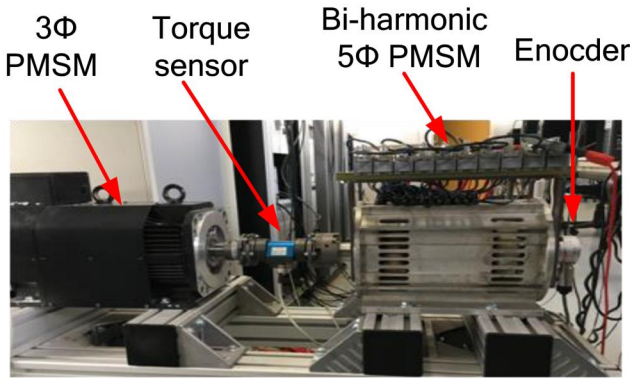
(a) Sinusoidal 5 ϕ PMSM coupled to 3 ϕ PMSM(b) Bi-harmonic 5 ϕ PMSM coupled to 3 ϕ PMSM

FIGURE 7 Details of the used two 5 – ϕ permanent magnet synchronous motor (PMSM) prototypes. (a) sinusoidal 5 ϕ PMSM coupled to 3 ϕ PMSM, (b) bi-harmonic 5 ϕ PMSM coupled to 3 ϕ PMSM

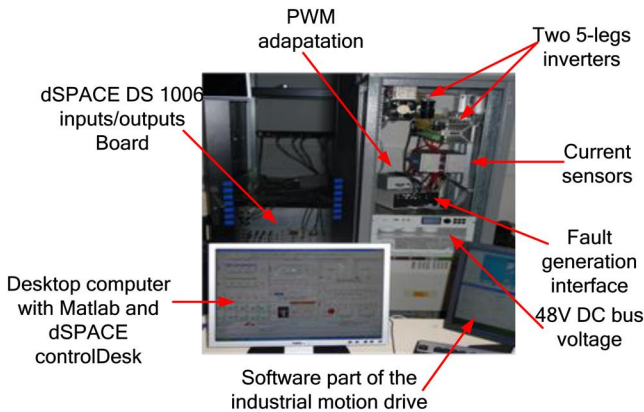


FIGURE 8 Overview of the power and control station

throughout the test. The fast transient process is conducted by a step increase of the rotor speed from 100 to 1000 rpm.

- **Test 2** – FDI process immunity against load change: The biharmonic 5 – ϕ PMSM is driven at a rotor speed equal to 1000 rpm. The transient states consist of two-step transitions of the load torque from no-load to 20 N.m, and then

TABLE 2 Parameters of the used 5 – ϕ PMSM

Technical data	Sinusoidal PMSM	Biharmonic PMSM
Resistance R (Ω)	0.0011	0.0324
Inductance of the main fictitious machine L_m (μ H)	118.5	101.3
Inductance of the second fictitious machine L_s (μ H)	51.4	152.7
Inductance of the zero sequence machine L_z (μ H)	110	4.5
Number of pole pairs	7	8
Amplitude of the fundamental harmonic of a speed-normalized back-EMF E_1 (V)	0.1358	0.1626
Amplitude of the third harmonic of a speed-normalized back-EMF E_3 in (%) of E_1	10%	122%
Amplitude of the fifth harmonic of a speed-normalized back-EMF E_5 in (%) of E_1	1.1%	0.7%

Abbreviations: EMF, electromotive forces; PMSM, permanent magnet synchronous motor.

from 20 N.m to no-load. As for the test 1, the MTPA control strategy is maintained so that $I_{r3} = 1.22 \times I_{r1}$.

- **Test 3** – FDI process effectiveness to detect open-switch fault: This test is performed on the sinusoidal 5 – ϕ PMSM prototype. The motor is driven in steady state at 1000 rpm. The value of the load is set to 20 N.m, giving $I_{r3} = 0.1 \times I_{r1}$.
- **Test 4** – FDI process effectiveness to detect open-phase fault: This test is conducted on the biharmonic 5 – ϕ PMSM prototype with the MTPA control. The rotor speed and the load torque are fixed at 1000 rpm and 20 N.m, respectively, giving $I_{r3} = 1.22 \times I_{r1}$.
- **Test 5** – FDI process capabilities to detect multiple open-phases fault in the VSI: This test is conducted on the biharmonic 5 – ϕ phase PMSM prototype. The reference speed is fixed at $N_r = 50$ rpm without load.

The results for test 1 are shown in Figure 9, which illustrates the time-domain waveforms of the rotor speed, the motor phase currents, and the diagnostic variables in normal operation mode. The rotor speed N_r is equal to 100 rpm until $t = 0.2$ s, then the value of N_r is linearly increased up to 1000 rpm at $t = 1.15$ s. For the fast transient and in steady state, it is observed that the phase currents always form a balanced five-phase system. The diagnostic variables D_n and I_n undergo a light variation but they remain always close to zero. Accordingly, the chosen threshold value of $T_{op} = 0.45$ and $T_{os} = 0.5$ can overcome the problem of false alarms in the FDI process. Therefore, the obtained results prove the high immunity against speed change of the proposed FDI process.

The results for test 2 are shown in Figure 10. It provides the time-domain waveforms of the rotor speed and the motor phase currents together with the diagnostic variables in the

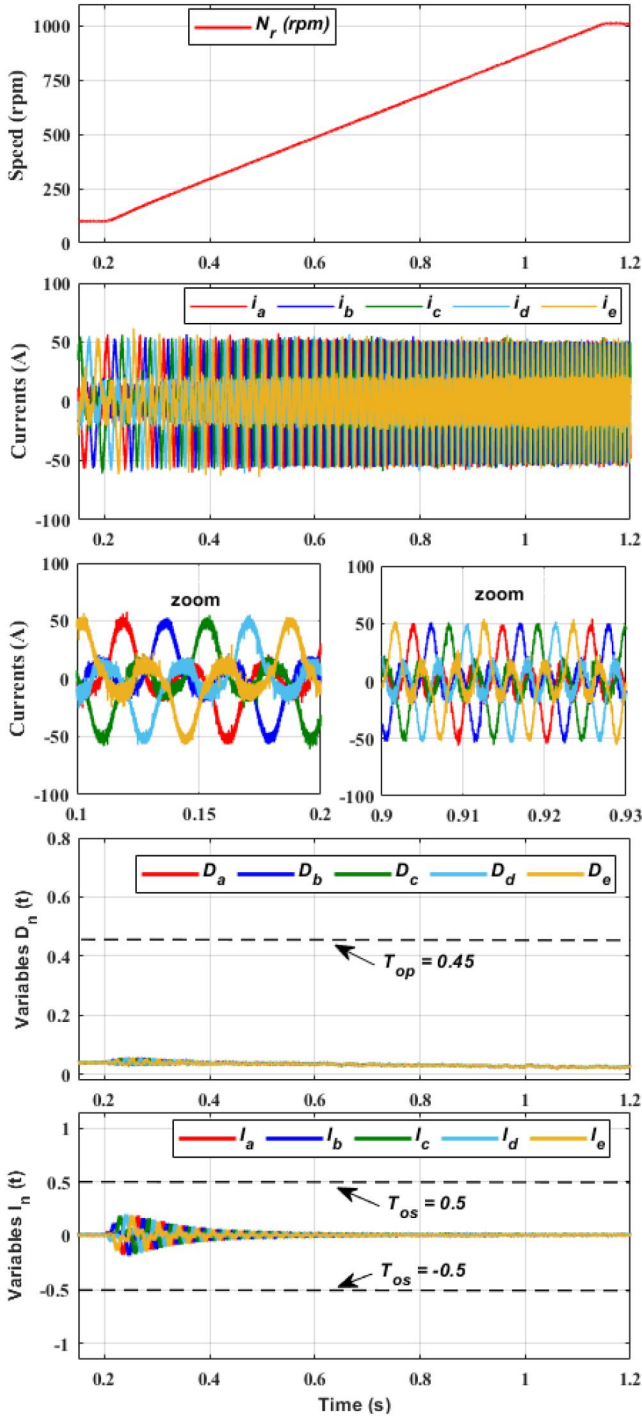


FIGURE 9 Test 1. Experimental results of the fault detection and identification process robustness. Time-domain waveforms of the rotor speed, the phase currents, and the diagnostic variables during rotor speed change from 100 rpm to 1000 rpm. $T_{em} = 20$ N.m (biharmonic 5- ϕ permanent magnet synchronous motor prototype)

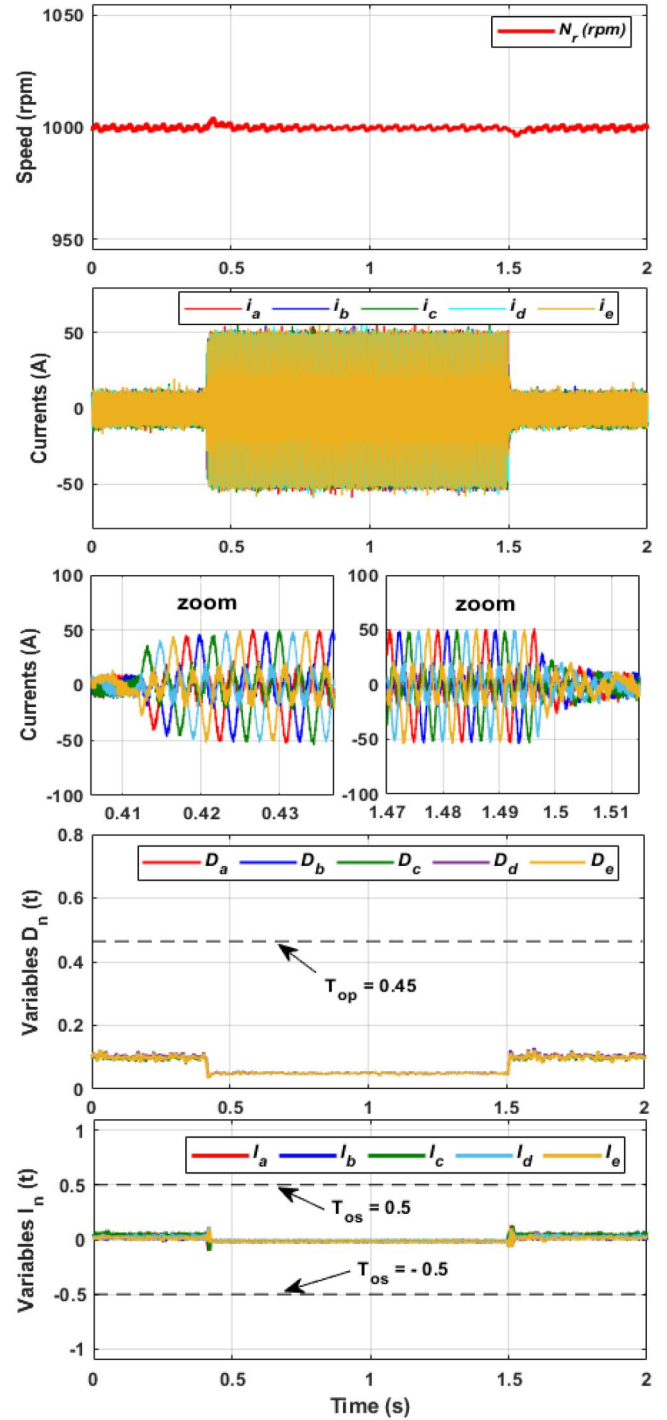


FIGURE 10 Test 2. Experimental results of the fault detection and identification process robustness. Time-domain waveforms of the rotor speed, the phase currents, and the diagnostic variables during load torque change from no-load to $T_{em} = 20$ N.m. $N_r = 1000$ rpm (biharmonic 5- ϕ permanent magnet synchronous motor prototype)

case of an abrupt change of the load torque from no-load to 20 N.m, and then from 20 N.m to no-load. Even though transient states are observed, the obtained results verify that the diagnostic variables are always around zero and within the ranges that correspond to a healthy operation mode of the

electric drive in both cases of transients. Once more, no false alarms are issued during these perturbations. These results prove the FDI process immunity against the fast transients due to load torque change.

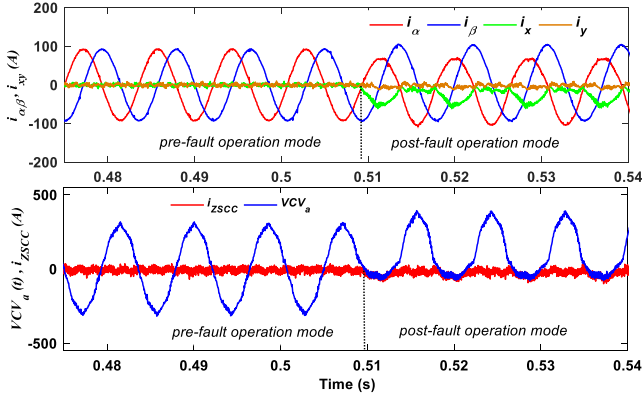


FIGURE 11 Test 3. Experimental results of the fault detection and identification process effectiveness. Time-domain waveforms of the current components $i_{\alpha\beta}$ and i_{xy} , the zero-sequence current component i_{zSCC} and the virtual current vector virtual current vector (VCV_a) before and after an open-switch fault in motor phase a. $T_{em} = 20$ N.m and $Nr = 1000$ rpm (sinusoidal 5 – ϕ permanent magnet synchronous motor prototype)

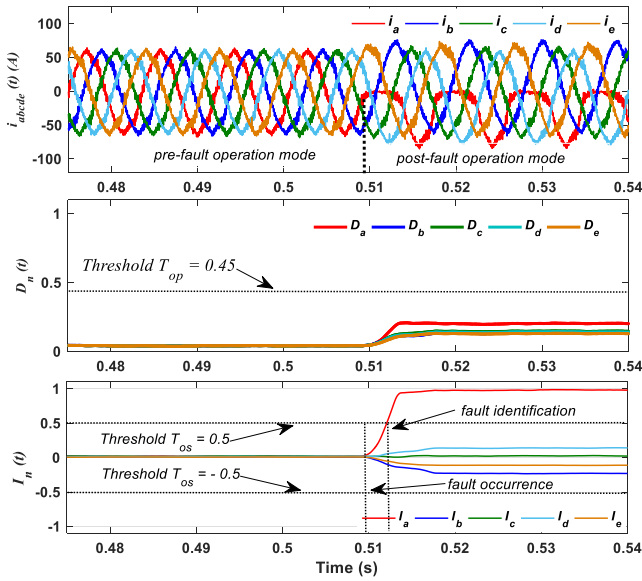


FIGURE 12 Test 3. Experimental results of the fault detection and identification process effectiveness. Time-domain waveforms of the motor phase currents, and the diagnostic variables D_n and I_n before and after an open-switch fault. $T_{em} = 20$ N.m and $Nr = 1000$ rpm (sinusoidal 5 – ϕ permanent magnet synchronous motor prototype)

Figures 11 – 12 illustrate the results for test 3. The behaviour of $i_{\alpha\beta}$ and i_{xy} together with the ZSCC i_{zSCC} and the virtual current vector VCV_a before and after the fault is shown in Figure 11. The i_{xy} are regulated to be zero in the case of sinusoidal 5 – ϕ PMSM prototype. In pre-fault operation mode, it can be seen that i_{zSCC} is very close to zero and VCV_a is much bigger than the value of the currents components. This gives zero values of the diagnostic variables as a result, D_n and I_n .

At $t = 0.5096$ s, an open-switch fault is applied to the VSI. After the fault occurrence, current i_a is limited to flow only in the negative direction (Figure 12). On the other side,

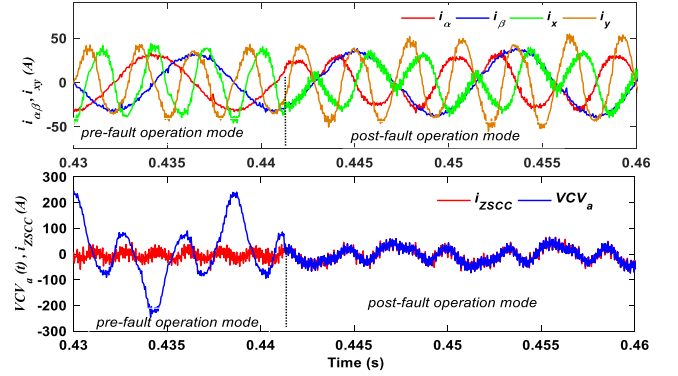


FIGURE 13 Test 4. Experimental results of the fault detection and identification process effectiveness. Time-domain waveforms of the current components $i_{\alpha\beta}$ and i_{xy} , the zero-sequence current component i_{zSCC} and the virtual current vector virtual current vector (VCV_a) before and after an open-phase fault of motor phase a. $T_{em} = 20$ N.m and $Nr = 1000$ rpm (biharmonic 5 – ϕ permanent magnet synchronous motor prototype)

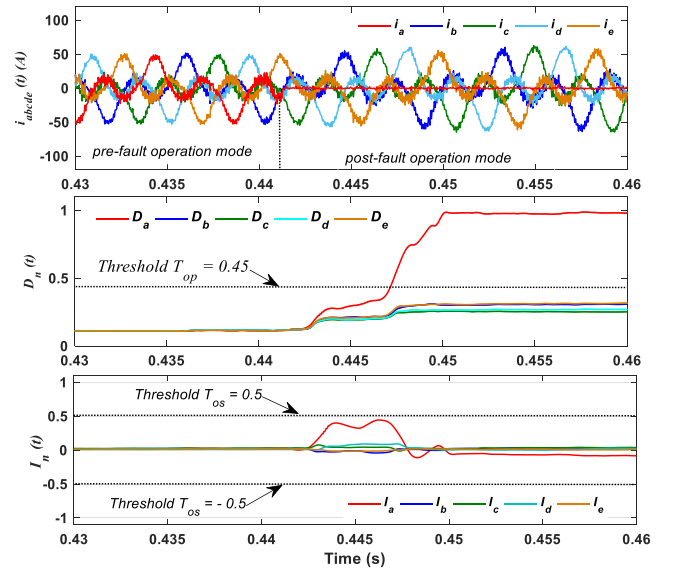


FIGURE 14 Test 4. Experimental results of the fault detection and identification process effectiveness. Time-domain waveforms of the motor phase currents, and the diagnostic variables D_n and I_n before and after an open-phase fault. $T_{em} = 20$ N.m and $Nr = 1000$ rpm. (biharmonic 5 – ϕ permanent magnet synchronous motor prototype)

the fault causes a significantly large variation of the virtual current vector VCV_a , which coincides with i_{zSCC} over a half current period, as predicted by Equation (13) and reported in Figure 11. As soon as the fault occurs, only the identification variable I_a exceeds the threshold $T_{os} = 0.5$ and converges to +1, indicating thus that the fault is an open-switch of T_1 in inverter-leg a. Regarding the diagnostic variables D_n , they undergo a light variation but are always less than the fixed threshold $T_{op} = 0.45$ used for open-phase fault detection. The state of these variables together with the variables I_n allowed a fast fault identification at $t = 0.5121$ s, taking 2.5 ms as a time delay (about 29% of the fundamental current period).

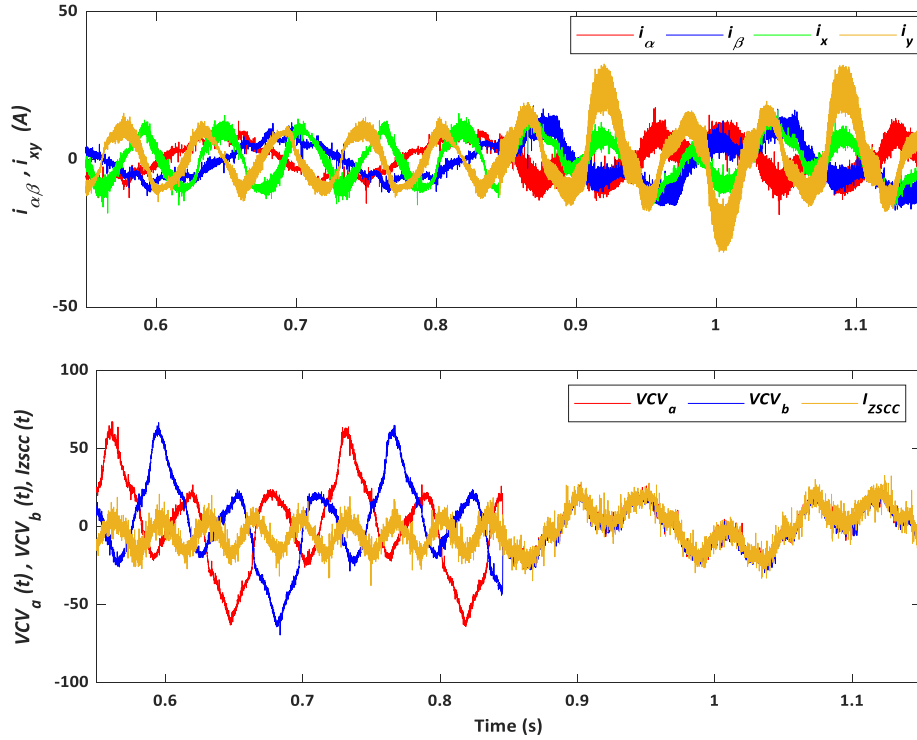


FIGURE 15 Test 5. Experimental results of the FDI process effectiveness. Time-domain waveforms of the current components $i_{\alpha\beta}$ and i_{xy} , the zero-sequence current component i_{zSCC} , and the virtual current vectors VCV_a and VCV_b before and after simultaneous open-phase fault of motor phases a and b. No-load and $N_r = 50$ rpm (biharmonic5 – ϕ PMSM prototype)

The results for test 4 are shown in Figure 13 – 14. Since this test is conducted on the biharmonic 5 – ϕ PMSM prototype, the phase currents contain fundamental and third harmonic components. That is why, in Figure 13, the values of i_{xy} are in the same order as $i_{\alpha\beta}$ ($I_{r3} = 1.22 \times I_{r1}$).

When the electric drive operates free of any fault, the measured phase currents form a balanced 5 – ϕ system, resulting in a near zero value of the ZSCC i_{zSCC} . The diagnostic variables D_n and I_n are therefore nearly zero and far from the fixed threshold values T_{op} and T_{os} . At $t = 0.4415$ s, the open-phase fault is applied to the motor phase a. As a result, current i_a suddenly drops to zero over the whole current period (Figure 14). In addition, a significantly large variation of the ZSCC i_{zSCC} is observed. In this case, i_{zSCC} coincides with the virtual current vector VCV_a over the current cycle (Figure 13), as predicted in Equation (12).

Since the open-phase fault occurred in motor phase a, the identification variable I_a undergoes a light variation over only a short-lived interval and then it drops to zero. As for the detection variable D_a , it can be seen that it increases immediately and exceeds the threshold $T_{op} = 0.45$. Based on the fact that the diagnostic variables I_n are equal to zero and only D_a reaches +1, the FDI process makes a decision that the fault is an open-phase fault in motor phase a. A fast fault detection therefore is accomplished at $t = 0.447$ s, taking a time delay of about 5.5 ms. Once more, the obtained results prove the capability of the proposed FDI process to detect an open-phase fault in the VSI.

Finally, the experimental results, shown in Figures 15–16, are for test 5, which illustrates the FDI process capabilities to detect multiple open-phase faults in the VSI. This test is conducted on the biharmonic 5 – ϕ phase PMSM prototype. The reference speed is fixed at $N_r = 50$ rpm without loading the motor. From a diagnostic point of view, this mode (low current magnitude and low rotor speed) can be considered a severe condition in which the performance of the proposed FDI process should be analysed. The measured phase currents present a significant harmonic distortion (Figures 15–16), which is a direct consequence of the sensors and switching noises. These sensors are designed to measure larger current values that can reach 250 A. Nonetheless, in pre-fault operation mode, the states of the diagnostic variables D_n and I_n , around zero, prove that the proposed FDI process is robust even under the considered extreme conditions.

The open-circuit fault is introduced simultaneously in phase a and phase b at $t = 0.848$ s. As a result, the motor phase currents i_a and i_b suddenly drop to zero over the whole current period. i_{zSCC} coincides simultaneously with the VCV_a and VCV_b over all current cycles (Figure 15). These results are in accordance with the predicted quantities in Equation (12). Regarding the diagnostic variables D_n , after the fault occurrence, only D_a and D_b increase immediately and converge to +1, whereas the variables D_c , D_d , and D_e assume values less than 0.2, far from the threshold $T_{op} = 0.45$. Similar to the previous cases, fast fault detection is achieved, in phase a and phase b, at $t = 0.911$ s.

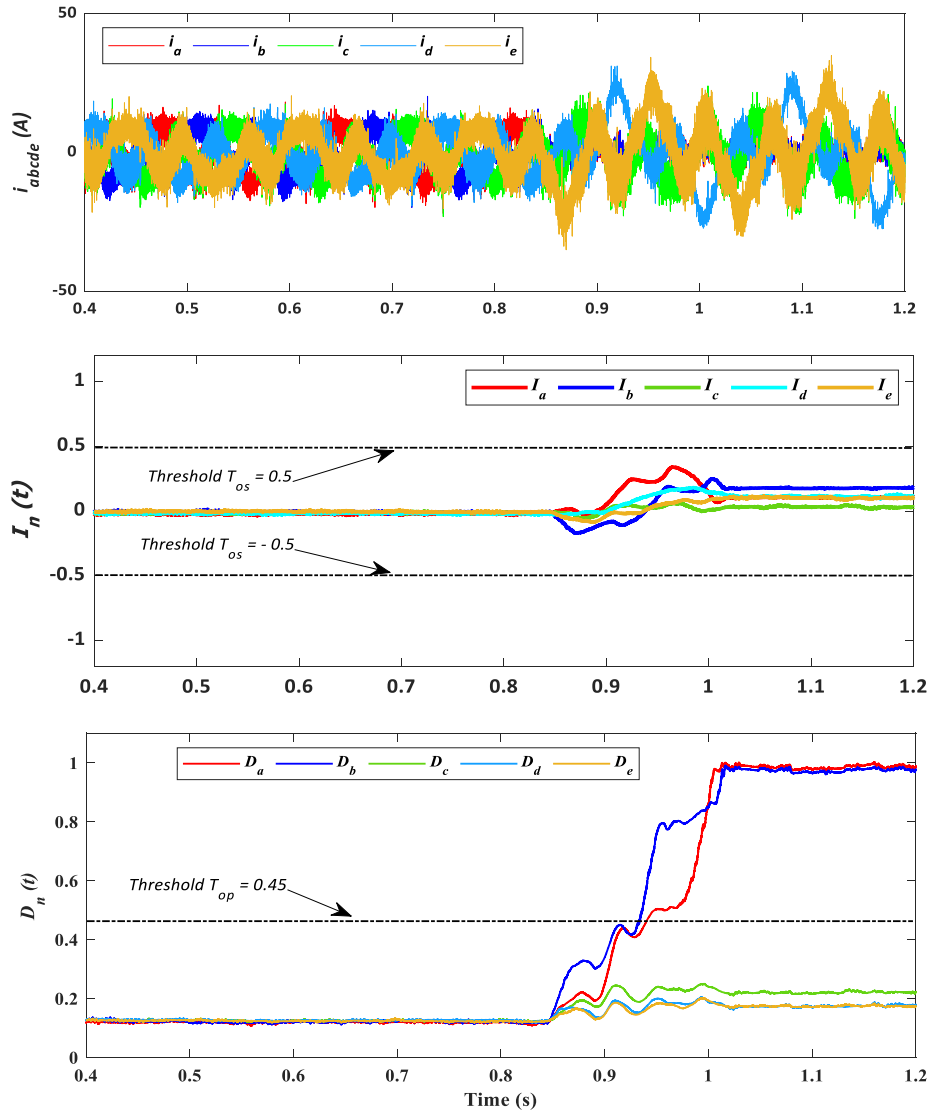


FIGURE 16 Test 5. Experimental results of the FDI process effectiveness. Time-domain waveforms of the motor phase currents, and the diagnostic variables D_n and I_n before and after simultaneous open-phase fault of motor phases a and b. No-load and $N_r = 50$ rpm (biharmonic 5- ϕ PMSM prototype)

The variables I_n assume zero values. These results are in accordance with the defined FDI process in this work. But here it should be noticed that the information given by the variables I_n is not interesting for this situation. Once more, the obtained results prove the high performance of the proposed algorithm even in extreme scenarios.

Finally, to conclude the high effectiveness of the proposed method under multiple faults, another test was also carried out in the case of two open-switch faults involving two different inverter legs. Once more, good effectiveness was obtained in this evaluation.

5 | CONCLUSION

In this paper, the development of a real-time inverter open-circuit fault diagnosis, where a signal-based approach is adopted for this purpose, has been presented. Adequate

variables, called virtual current vectors, are defined and used together with the ZS current component to design the FDI process. The diagnostic steps have been performed by a direct projection of the ZSCC onto the defined V_{CV_n} . Two simple fault indices are used to detect and identify the single and multiple open-switch and open-phase faults in the electric drive.

The proposed method has been conducted only on a 5-leg inverter feeding 5- ϕ PMSM, but it can be applied to other multiphase machines owning a path for the ZSCC. It uses current sensors that are already available on the electric drive without additional hardware. Two different 5- ϕ PMSM prototypes—sinusoidal and biharmonic PMSM—are used to verify the independence of the proposed approach of the transient states and to validate its feasibility. The obtained results confirm the effectiveness and the robustness of the proposed method and its capability to detect the single and multiple open-switch and open-phase faults.

In comparison with similar diagnostic methods that are applied to multiphase PMSM drives, the proposed method here allows significant reduction in computational load through an algorithm simpler than those employed in [32, 33], especially in terms of required number of operations. This simplification is obtained by taking advantage of VCVn, which is simply obtained from the motor phase currents in α - β and x-y frames, and by avoiding RLS identification algorithm and complex trigonometric functions operations. In addition, the proposed method achieves robustness and effectiveness in the diagnosis for the case of the biharmonic multiphase PMSMs in comparison with the methods presented in [31, 33, 34], which are limited to sinusoidal machines supplied by sinusoidal currents. Finally, in comparison with the methods based on ZSCC as given in [36, 37], the proposed FDI process detects the open-switch (single and multiple) and the open-phase faults even in the presence of ZS current component in normal operation mode.

ACKNOWLEDGMENTS

Part of this work was achieved within the framework of CE2I project. CE2I is co-financed by European Union with the financial support of European Regional Development Fund (ERDF), French State and the French Region of Hauts-de-France.

ORCID

Mohamed Trabelsi  <https://orcid.org/0000-0001-6904-8756>
Eric Semail  <https://orcid.org/0000-0001-8565-1707>

REFERENCES

- Levi, E.: Multiphase electric machines for variable-speed applications. *IEEE Trans Ind Electron.* 55(5), 1893–1909 (2008)
- Huang, X., et al.: Design of a five-phase brushless DC motor for a safety critical aerospace application. *IEEE Trans. Indus. Electron.* 59(9), 3532–3541 (2012)
- Cao, W., et al.: Overview of electric motor technologies used for more electric aircraft (MEA). *IEEE Trans Ind Electron.* 59(9), 3523–3531 (2012)
- Patel, V.I., et al.: Six-phase fractional-slot-per-pole-per-phase permanent-magnet machines with low space harmonics for electric vehicle application. *IEEE Trans. on Ind. Applicat.* 50(4), 2554–2563 (2014)
- Parsa, L., Toliyat, H.A.: Fault-tolerant interior-permanent-magnet machines for hybrid electric vehicle applications. *IEEE Trans Veh Technol.* 56(54), 1546–1552 (2007)
- Mekri, F., Ben Elghali, S., Benbouzid, M.E.H.: Fault-tolerant control performance comparison of three- and five-phase PMSG for marine current turbine applications. *IEEE Trans. Sustain. Energy.* 4(2), 425–433 (2013)
- Hanna, R.A., Prabhu, S.: Medium-voltage adjustable-speed drives-users' and manufacturers' experiences. *IEEE Trans. on Ind. Applicat.* 33(6), 1407–1415 (1997)
- Bin, L., Sharma, S.K.: A literature review of IGBT fault diagnostic and protection methods for power inverters. *IEEE Trans Indus. Appl.* 45(5), 1770–1777 (2009)
- Nguyen, N.K., et al.: Fault-tolerant operation of an open-end winding five-phase PMSM drive with short-circuit inverter fault. *IEEE Trans Ind Electron.* 63(1), 595–605 (2016)
- Guzman, H., et al.: Comparative study of predictive and resonant controllers in fault-tolerant five-phase induction motor drives. *IEEE Trans Ind Electron.* 63(1), 606–617 (2016)
- Vu, D.T., et al.: Control strategies for non-sinusoidal multiphase PMSM drives in faulty modes under constraints on copper losses and peak phase voltage. *IET Electr Power Appl.* 13(11), 1743–1752 (2019)
- Tani, A., et al.: Control of multiphase induction motors with an odd number of phases under open-circuit phase faults. *IEEE Trans Power Electron.* 27(2), 565–577 (2012)
- Bermudez, M., et al.: Open-phase fault-tolerant direct torque control technique for five-phase induction motor drives. *IEEE Trans Ind Electron.* 64(2), 902–911 (2017)
- Li, Q., et al.: Fault-tolerant drive system based on the redundancy bridge arm for aerospace applications. *IET Electr Power Appl.* 2(6), 780–786 (2017)
- Jung, S.M., et al.: An MRAS-based diagnosis of open-circuit fault in PWM voltage-source inverters for PM synchronous motor drive systems. *IEEE Trans Power Electron.* 28(5), 2514–2526 (2013)
- Jlassi, I., et al.: A robust observer-based method for IGBTs and current sensors fault diagnosis in voltage-source inverters of PMSM drives. *IEEE Trans. on Ind. Applicat.* 53(3), 2894–2905 (2017)
- Campos-Delgado, D.U., Espinoza-Trejo, D.R.: An observer-based diagnosis scheme for single and simultaneous open-switch faults in induction motor drives. *IEEE Trans Ind Electron.* 58(2), 671–679 (2011)
- Arashloo, S., et al.: Observer-based open transistor fault diagnosis and fault-tolerant control of five-phase permanent magnet motor drive for application in electric vehicles. *IET Power Electron.* 8(1), 76–87 (2015)
- Maamouri, R., et al.: Mixed model-based and signal-based approach for open-switches fault diagnostic in sensorless speed vector controlled induction motor drive using sliding mode observer. *IET Power Electron.* 12(5), 1149–1159 (2019)
- Estima, J.O., Marques Cardoso, A.J.: A new algorithm for real-time multiple open-circuit fault diagnosis in voltage-fed PWM motor drives by the reference currents errors. *IEEE Trans. Indus. Electron.* 28(5), 3496–3505 (2013)
- Estima, J.O., Marques Cardoso, A.J.: A new approach for real-time multiple open-circuit fault diagnosis in voltage-source inverters. *IEEE Trans. on Ind. Applicat.* 47(6), 2487–2494 (2011)
- Meinguet, F., et al.: A method for fault detection and isolation based on the processing of multiple diagnostic indices: application to inverter faults in AC drives. *IEEE Trans Veh Technol.* 62(3), 995–1009 (2013)
- Santos Moraes, T.J., et al.: Inverter fault diagnosis of an electrical series-connected two sinusoidal six-phase permanent magnet machines drive. *IET Electr Power Appl.* 14(8), 1412–1420 (2020)
- Trabelsi, M., Boussak, M., Gossa, M.: PWM-Switching pattern-based diagnosis scheme for single and multiple open-switch damages in VSI-fed induction motor drives. *ISA (Instrum Soc Am) Trans.* 51(2), 333–344 (2012)
- De Araujo Ribeiro, R.L., et al.: Fault detection of open-switch damage in voltage-fed PWM motor drive systems. *IEEE Trans Power Electron.* 18(2), 587–593 (2003)
- Zhang, H., et al.: Voltage vector error fault diagnosis for open-circuit faults of three-phase four-wire active power filters. *IEEE Trans Power Electron.* 32(3), 2215–2226 (2017)
- Gao, Z., Cecati, C., Ding, S.X.: A survey of fault diagnosis and fault-tolerant techniques-part I: fault diagnosis with model-based and signal-based approaches. *IEEE Trans Ind Electron.* 62(6), 3757–3767 (2015)
- Scuiller, F., Zahr, H., Semail, E.: Maximum reachable torque, power and speed for five-phase SPM machine with low armature reaction. *IEEE Trans Energy Convers.* 31(3), 959–969 (2016)
- Gong, J., et al.: Design considerations of five-phase machine with double p/3p polarity. *IEEE Trans Energy Convers.* 34(1), 12–24 (2019)
- Trabelsi, M., Semail, E., Nguyen, N.K.: Experimental investigation of inverter open-circuit fault diagnosis for biharmonic five-phase permanent magnet drive. *IEEE J. Emerg. Sel. Topics Power Electron.* 6(1), 339–351 (2018)
- Duran, M.J., et al.: A simple, fast and robust open-phase fault detection technique for six-phase induction motor drives. *IEEE Trans Power Electron.* 33(1), 547–557 (2018)

32. Salehifar, M., et al.: Fault detection and fault tolerant operation of a five phase PM motor drive using adaptive model identification approach. *IEEE J. Emerg. Sel. Topics Power Electron.* 2(2), 212–223 (2014)
33. Trabelsi, M., Nguyen, N.K., Semail, E.: Real-time switches fault diagnosis based on typical operating characteristics of five-phase permanent magnetic synchronous machines. *IEEE Trans. Indus. Electron.* 63(8), 4683–4694 (2016)
34. Gonzalez-Prieto, I., et al.: Open-switch fault detection in five-phase induction motor drives using model predictive control. *IEEE Trans Ind Electron.* 65(4), 3045–3055 (2018)
35. Trabelsi, M., et al.: Open-switch fault effects analysis in five-phase PMSM designed for aerospace application. In: *Proc. Of IEEE-SPEEDAM. Italy* (2016)
36. Hang, J., et al.: Open-Phase Fault Detection in delta-connected PMSM drive systems. *IEEE Trans Power Electron.* 33(8), 6456–6460 (2018)
37. Shahin, A., Martin, J.P., Pierfederici, S.: Zero-sequence current based diagnostic method for open-switch fault detection in parallel inverters system. *IEEE Trans Power Electron.* 34(4), 3750–3764 (2019)
38. Zhan, H., Zhu, Z.Q., Odavic, M.: Analysis and suppression of zero sequence circulating current in open winding PMSM drives with common DC bus. *IEEE Trans. on Ind. Applicat.* 53(4), 3609–3620 (2017)
39. Karampuri, R., Jain, S., Somasekhar, V.T.: Sample-averaged zero-sequence current elimination PWM technique for five-phase induction motor with opened stator windings. *IEEE J. Emerg. Sel. Topics Power Electron.* 6(2), 864–873 (2018)

How to cite this article: Trabelsi M, Semail E. Virtual current vector-based method for inverter open-switch and open-phase fault diagnosis in multiphase permanent magnet synchronous motor drives. *IET Electr. Power Appl.* 2021;1–16. <https://doi.org/10.1049/elp2.12083>